Appendix A

Numerical modelling of dynamic recrystallization using Elle: Description of the model

A1 General approach

The modelling system Elle is designed to model the two-dimensional evolution of a microstructure that is a result of several concurrent micro-processes. Numerical modelling of several concurrent processes results in a nonlinear problem. Complex algorithms and differential equations would have to be employed if the different equations which each describe the microstructural change according to one individual process should be solved simultaneously. So far, such algorithms are largely lacking.

Another approach is taken with Elle. It is assumed that a fabric is a result of microstructural changes due to process a, b, c, …, n, and that the fabric development can be simulated by the sum of the microstructural changes of each of the individual processes according to the general relationship

$$\delta f(a, b,..., c) = \delta f(a) + \delta f(b) + ... + \delta f(c) \qquad \text{(Eq. A1)}$$

Equation A1 is only given if each process can be discretized in space and time. In Elle Eq. A1 is valid as processes operate at a very small scale and only for a small time increment.

This approach which describes the nonlinearity of the problem by discretization of the problem into distinct, linear and small segments in space, time and process, may lead to some inaccuracy of results. Nevertheless, right now, there is no other numerical model available that simulates the different simultaneously active processes needed for simulations of dynamic recrystallization.

A2 General description of modelling environment used

The modelling system Elle (Evans et al., 2000; Jessell et al., 2001) is based on a data structure that describes a polycrystalline material using a two-dimensional network of nodes and connecting boundaries at the grain scale (Fig. A2). The network of nodes and boundaries forms a square unit cell with periodic boundaries. Individual nodes possess attributes of position and topology and may have additional attributes such as chemistry and stress state. The polygonal domains defined by these nodes and their connecting boundaries may possess attributes such as mineralogy, viscosity, strain, stress, dislocation density, age and lattice orientation. Each polygon has an attribute which specifies if the polygon is a true grain or if it is part of a larger grain; hence a subgrain. The specific distinction between grain and subgrain will be described in detail in section A3.5. Data on the geometry of the structure and values of nodes and polygons are stored in an Elle data file. To simulate the progress of a process, distinct process algorithms can interact with this data structure (a) by using it to determine the local values of driving forces, (b) by repositioning, creation and removal of nodes, (c) by reconnecting boundary segments, and (d) by altering attributes. A central shell program controls the evolution of extrinsic variables, such as temperature, and determines which micro-processes will be involved by controlling the order and rate of execution of individual process algorithms (Fig. A3a).

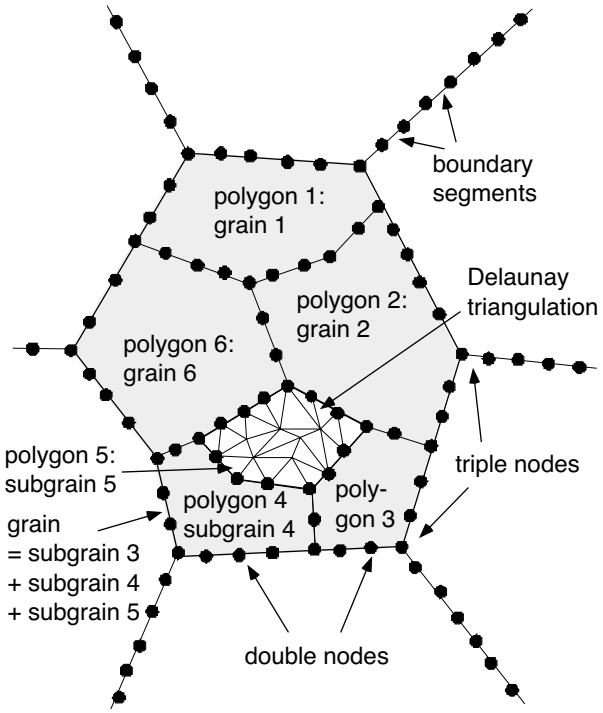

Figure A2 *Representation of the 2-dimensional finite element map of a grain aggregate. Each polygon domain (grain; polygon 1, 2, 6, 7) can be subdivided into a number of polygonal subdomains (subgrains; polygon 3, 4, 5), each of which in turn has a number of properties assigned to them, such as crystal lattice orientation. All polygons can be if desirec triangulated to smaller elements using a Delaunay triangulation routine. This triangulation is, in contrast to the polygons, nodes and boundary segments, not permanent aud can be used temporarily e.g. for the subgrain formation routine (ELLE_SPLIT; see text). Triangulation elements may also have individual properties, including the stress and strain state during deformation, and/or trace element concentration..*

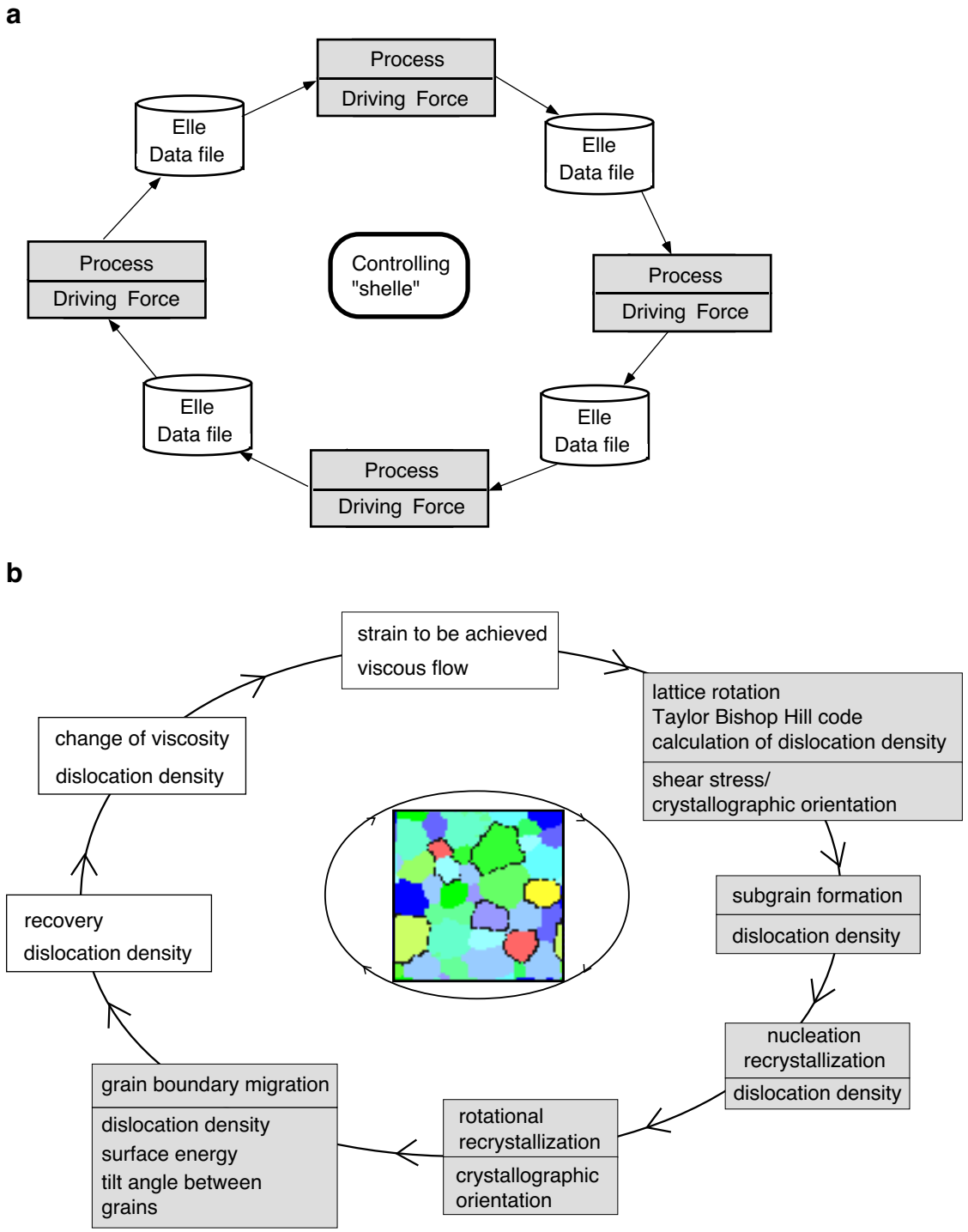

Figure A3 ***(a)*** *General schematic flow diagram of the Elle modelling system.* ***(b)*** *Flow diagram of the dynamic recrystallization model. Processes given in the white boxes are those which have no true driving force (e.g. calculation of viscosity), while processes (top of box) and driving forces (bottom of boxes) are depicted in grey boxes.*

In the model plane strain deformation of a viscous material, crystallographic rotation, formation of subgrains, recrystallization by nucleation, rotational recrystallization, grain boundary migration and recovery is simulated (Fig. A3b).

To implement real world values in the model and to translate the calculated numerical values to real world values several scaling factors are needed. Scaling factors which need to be specified are the time (t_{scale}), length (l_{scale}), dislocation density (ρ'_{scale}) and the stress (τ_{scale}). To specify the spatial resolution of the node-boundary mesh a minimum and maximum node separation and a so called *SwitchDistance* has to be chosen which control the computational minimum and maximum separation of nodes and minimum distance for adjacent triple nodes, respectively (Fig. A4).

Routines that simulate individual processes are described below. In these routine descriptions there is first a section on the general background of the microstructural process and a second section on how the routine works in the Elle. Routine names are written in CAPITAL LETTERS, functions in **bold** and variables specific to the Elle model in *italics*. In Tab. A1 used symbols are listed (end of this file).

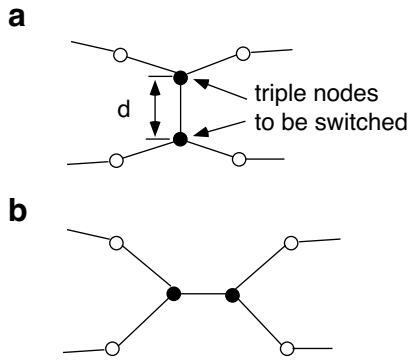

Figure A4 *Schematic illustration of a NeighbourSwitch; here a so-called T1-event (Weaire & Rivier, 1984). If a node is a triple junction and if any of the neighbours within the minimum distance d (SwitchDistance) are triples, the node will triple-switch with its closest triple neighbour.*

A3 Description of individual processes

A3.1 Viscous deformation (BASIL)

Viscous deformation is modelled by the program BASIL (Barr and Houseman, 1992; Barr and Houseman, 1996), which uses a finite element method to calculate stress and strain in linear and non-linear incompressible viscous, non-elastic materials, up to strains of the order of 100%. The calculations describe viscous Earth materials that undergo irreversible large-strain deformation under the influence of body forces and surface tractions. The program permits a spatially variable Newtonian or non-Newtonian viscosity in a 2-D geometry with traction and/or velocity boundary conditions. The 2-D deformation field represents either plane strain deformation, or it permits a specified distribution of normal stress in the third direction. In Elle plane stress calculations are used, which result in a special case of a thin viscous sheet formulation. The observation surface corresponds to the xy-plane of a sheared rock (Fig. A5). The type of plane strain deformation of the unit cell in terms of the kinematic vorticity number W_n (Means et al., 1980) and boundary conditions are defined by the user. The program can either simulate the movement of two pistons at top and bottom of the model or movement according to a set of velocity vectors at all points of the cell boundaries. To model deformation with pistons, the displacement of the 4 corners of the cell per time step are defined by the user. Otherwise the minimum and maximum values of the finite element node velocity components are defined. The Elle microstructure will be distorted into a parallelogram during deformation. The square unit cell can be regained by repositioning nodes that are outside the unit cell. To be able to do this two prerequisites have to be met: (a) the mesh of nodes and node-to-node-boundaries must be a unit cell structure with periodic boundaries (i.e. it wraps around in the x- and y-

direction) and (b) the simulated deformation must have been simple shear. To visualize and to check if the values calculated by BASIL are reasonable a display program (SYBIL) is provided (Barr and Houseman, 1996). SYBIL reads the solution files, and enables the user to plot selected quantities in the form of contour plots of strain, stress or displacement quantities, arrow plots of vectors of principal stresses, mesh plots or other derived quantities.

This deformation routine has been shown to be valid for modelling viscous deformation of linear and non-linear viscous materials (Barr and Housemann, 1992; Barr and Housemann, 1996; Bons et al., 1997)

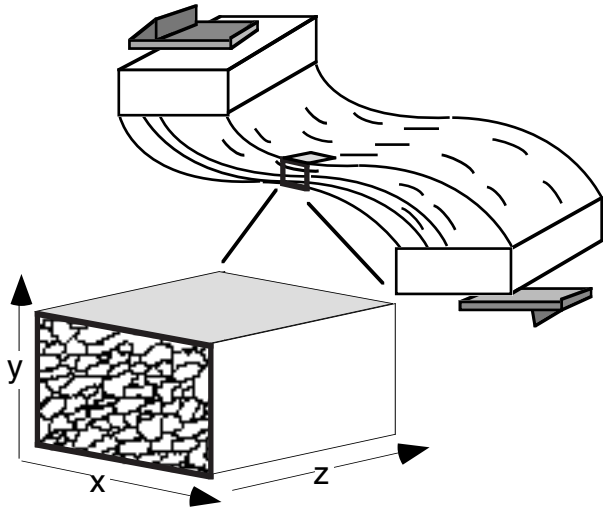

Figure A5 *Schematic diagram of sheared rock, orientation of x, y, z axis and observation surface (xy-plane) in numerical simulations.*

A3.2 Lattice rotation and accumulation of dislocations (ELLE_TBH)

One of the basic deformation mechanisms in most crystals is crystallographic slip, which involves the movement of dislocations in certain planes and directions in each crystal which gives rise to the rotation of the crystal during deformation (e.g. Weiss and Wenk, 1985 and references therein; Law, 1990). For a given crystal structure there are well-defined combinations of planes and directions in which slip occurs. For example, in the case of quartz, slip can occur on the {001} plane (i.e. the basal plane) and in the <100> directions (i.e. parallel to the a-axes). (e.g. Hobbs, 1985 and references therein), but also in several other direction on different planes.

The occurrence of crystallographic slip during plastic deformation gives rise to two phenomena. One phenomenon that occurs is the rotation of the crystal lattice during deformation (Taylor, 1938; Bishop and Hill, 1951a, 1951b; Lister and Paterson, 1979). The crystal rotation is required for accommodating an arbitrary deformation because deformation by slip is possible only along a small number of slip systems. The other phenomenon is the increase in dislocation density during deformation due to the built up of tangles (locks) within the crystal. These tangles arrest further movement of dislocations. Because the resistance to dislocation movement increases in the presence of the locks, the crystal requires additional stress in the slip system to move further dislocations, and the crystal is said to ”work-harden” (Kocks et al., 1975; Kocks, 1976; Mecking and Kocks, 1981; Barber, 1985). Entanglement of dislocations is one of the mechanisms by which the deformation energy is stored within the crystal. The microstructure of the work-hardened material consists of a large number of cells, or subgrains, whose boundaries are essentially composed of a dense wall of dislocations (see section A3.3).

ELLE_TBH consists of two parts. The first part is the calculation of the crystal lattice rotation and the associated work (Taylor Bishop Hill calculations; Taylor, 1938; Bishop and Hill, 1951a, 1951b; Lister and Paterson, 1979) and the second part the calculation of the accumulation of dislocations. For the Taylor Bishop Hill calculations several assumptions are made. (a) Dislocation glide is the only deformation mechanism and each grain (smallest order polygons) deforms homogeneously to same strain. This is an approximation to nature where crystals deform heterogeneously (e.g. mica deform by sliding on its basal planes). (b) Each grain has at least 5 independent slip systems (known as the von Mises criterion (von Mises, 1928)). (c) The activity on any one slip system results in a small increment of simple shear parallel to the slip plane in the direction of the slip vector. Until the entire strain increment can be achieve for a grain, no deformation takes place at all, so the stress gradually increases until the critical resolved shear stress (CRSS) threshold is surpassed on just enough slip systems to allow the specific strain to take place (Lister et al., 1978; Jessell and Lister, 1990). Once this state is achieved, the work term can be calculated as the products of the small strains achieved by each slip system and the imposed stress. (d) No lattice reorientation due to rigid body rotation is taken into account and strain is assumed to be plane strain.

The Taylor Bishop Hill routine was developed by Lister et al. (1978), further developed by Jessell and Lister (1990), and later modified to match the needs of the Elle project by Mark Jessell. Inputs for this process are crystal symmetry and slip system definition with CRSS values for a given mineral species. According to the CRSS values and the stress tensors provided by BASIL, the new crystal orientation and the work necessary to achieve this crystallographic lattice rotation are calculated.

For the second part of ELLE_TBH the following considerations have to be taken into account. A general positive correlation of dislocation density and differential stress is predicted from theory (Kohlstedt and Weathers, 1980) and observed in experiments (e.g. Durham et al., 1977; Beemann and Kohlstedt, 1988; De Bresser, 1996). At steady state the relationship between dislocation density and stress is given by

$$\rho = K(\sigma/|b|)^2 \qquad \text{(Eq. A2)}$$

(Argon, 1970), where ρ is the density of mobile dislocations, K a constant, σ stress and $|b|$ the magnitude of the Burgers vector of the dislocation.

In ELLE_TBH, the change in dislocation density is assumed to be linearly proportional to the amount of work per unit area.

The new dislocation density (ρ'_{new}) of a polygon undergoing work is calculated according to the following equation

$$\rho'(new) = a \bullet \rho'(initial) + b \bullet \ ework \qquad \text{(Eq. A3)}$$

where a and b are constants. Additionally, $a+b$ =1.1 to ensure an increase of dislocations with progressive deformation (Fig. A6). $\rho'(initial)$ corresponds to the "initial" dislocation density of a polygon given in the Elle data file before the onset of ELLE_TBH and *ework* the calculated work for deformation of the grain according to the Taylor Bishop Hill code (for more details see Lister et al., 1978; Jessell and Lister, 1990). The calculated $\rho'(new)$ of the relevant polygon is written to the new Elle data file. If one simply uses a direct function of the *ework* without any reference the previous dislocation density, a strong oscillation of dislocation density occurs. Grains with high dislocation density (i.e. high viscosity; section A3.7) in one time step will do little work and hence will have low dislocations densities (i.e. viscosities) in the next time step.

The part of the routine that is used to calculated the crystallographic rotation and work term have been shown to be relevant to rock deformation by Lister et al. (1978) and Jessell and Lister (1990).

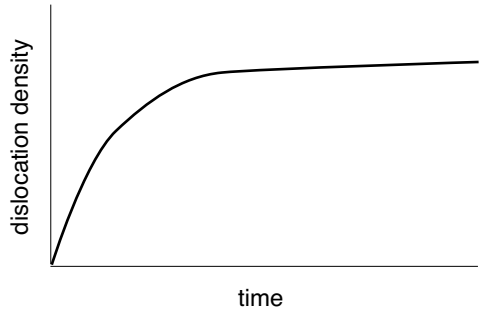

Figure A6 *Graph of the increase of dislocation density with time assuming a time-independent value for the work necessary to deform a grain.*

A3.3 Formation of subgrains (ELLE_SPLIT)

During deformation dislocations are generated and stored in a crystal. Dislocations do not occur in thermodynamic equilibrium and tend to move to lower the energy of the system (Barber, 1985 and references therein; Gottstein and Svindlerman, 1999 and references therein). One way to minimize the free energy of dislocations is the rearrangement of dislocations in low energy dislocation structures such as planar dislocation arrays (tilt walls, cell walls, subgrain walls) (e.g. Gottstein and Mecking, 1985; Kocks, 1985). Such arrays show dislocations of one sign at one side of a wall and of the other sign at the other side (Gottstein and Mecking, 1985 and references therein). First, the cell walls sharpen, until they become subgrain boundaries, then the substructure coarsens (Sandström, 1977; Gottstein and Mecking, 1985; Kocks, 1985; Gottstein and Svindermann, 1999, and references therein). An increase in the number of dislocations results in an increase in internal stresses. These stresses inside the developing cells provide the local driving force for rearrangement of dislocations in tilt walls (Kocks, 1985). Therefore, it is assumed that the higher the dislocation density the higher the possibility that dislocations arrange themselves in such tilt walls (Barber, 1985; Kocks, 1985). At the first for-

mation of subgrain boundaries the new subgrains have a similar dislocation density because the original grain as the dislocations are only rearranged but not annealed (e.g. Kocks, 1976). The size of the new subgrains size is characteristic for a mineral species (e.g. Twiss, 1977; Kohlstedt and Weathers, 1980; Christie et al., 1980; Kronenberg and Tullis, 1984).

The subgrain formation routine ELLE_SPLIT performs ”splitting” i.e. subdivision of a polygon into several new polygons. Accordingly, it models the discontinuous development of subgrain boundaries. Although such a model is a simplification of the mechanism of subgrain boundary formation in nature, cell walls evolve to coarse subgrain walls that can be recognized macroscopically only as subgrain but not cell walls. The driving force $F(\rho)$ for subgrain formation is the total strain energy per unit area in the used two dimensional model. In the used node network this is the energy per node. $F(\rho)$ is calculated according to

$$F(\rho) = \rho' \bullet \rho_{energy} \bullet \rho'_{scale} \qquad \text{(Eq. A4)}$$

where ρ' is the dislocation density, ρ_{energy} the energy of dislocations and ρ'_{scale} the dislocation density scaling factor. If $F(\rho) > Th_{split}$ (threshold value for splitting of a polygon), the grain has a probability to ”split” into subgrains. The probability for "splitting" increases with increasing $F(\rho)$ and is determined according to the probability function $\mathbf{P_{action}}$.

```
test_threshold=action_threshold/ F(ρ);
                    /* for high values of F(ρ) the test_threshold is small and vice versa */
test=drand48();
                    /* randomly picked number between 0 and 1 */
if (test>test_threshold) CallForAction                    (Eq. A5)
```

where *action_threshold* (e.g. Th_{split}) is the energy threshold value for a certain action (e.g. splitting) defined by the user. The function drand48() belongs to a family of functions that generate pseudorandom numbers using the linear congruential algorithm and 48-bit integer arithmetic. The drand48( ) function returns a random non-negative, double-precision, floating-point value between 0 and 1.0. **CallForAction** is a function that calls a certain action such as the splitting of a polygon. This probability function is also used for the probability for recrystallization by nucleation (section A3.4).

The division of a ”parent” polygon into several smaller polygons (i.e. subgrains) is done by successive splitting of one ”parent” polygon into two smaller ”daughter” polygons. The boundary between the new ”daughter” polygons is found in the following way. First, the "parent" polygon is triangulated according to the Delaunay triangulation routine (Shewchuk, 1996). A direction vector of a preferred direction of splitting O is specified either according to a certain probability to be in a specified orientation relative to the crystallographic axes of the ”parent” polygon or by a random number generator. The direction of the different triangulation legs joined to the starting node at the "parent" boundary is compared with the given direction vector. The triangulation leg that has the smallest angle with O and forms an angle above 45 degrees with the ”parent” polygon boundary is chosen for the first part of the splitting-walk (Fig. A7). The next triangulation leg used for the splitting-walk (new subgrain boundary) is again chosen according to its angle with the direction vector. Once the splitting-walk arrives at the boundary of the "parent" polygon the size of the resultant two "daughters" is calculated. If one of the resultant polygons is smaller than the given minimum area (*MinArea*) the walk is

rejected and a new splitting-walk is attempted starting from another boundary node. If the area of a ”daughter” polygons is above the maximum polgyon area (*MaxArea*) it is split again into another set of ”granddaughter” polygons. The range of subgrain size (*MinArea* < subgrain size < *MaxArea*) is defined by the user and is assumed to be characteristic for a mineral species. Most of the attributes of the ”parent” (e.g. mineral species, dislocation density) are passed on to the ”daughters”. Additionally, the two daughters are marked as subgrains (split attribute = 1) and are given the same grain number attribute which specifies them as subgrains of a larger grain (see Fig. A2).

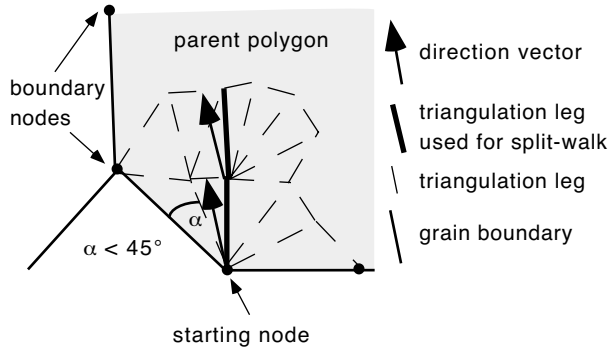

Figure A7 *Schematic diagram of the determination of the “splitting-walk” along triangulation legs.*

A3.4 Recrystallization by nucleation (ELLE_NUCLXX)

In many natural examples e.g. albite, magnesium, quartz (Knipe and White, 1979; Ion et al, 1982; Fitz Gerald et al., 1983; Tullis and Yund, 1985, Urai et al. 1986; Drury and Urai, 1990) subgrains show distinct discontinuous stages where the dislocation structure in a subgrain is cleared out producing relatively strain- and dislocation-free grains (regime D in Fig. A1). In contrast to geology, in metallugy this process is commonly referred to as dynamic recrystallization (Hardwick et al., 1961; Stüwe, 1965; Nicholis and McCormick, 1970; Gottstein and Mecking, 1985). A subgrain that has a high dislocation density is characterized by a high number of even smaller subgrains (cells) to very small scales (μm) which themselves have low internal dislocation density values (Kocks, 1985). One of these minute cells can act as a new nucleus, that will grow rapidly at the cost of its neighbouring cells (Fig. A8a; Gottstein and Mecking, 1985; Gottstein and Svindlerman, 1999, and references therein). Three prerequisites have to be fulfilled to allow such a nucleation: (1) the total free energy must decrease during expansion of the nucleus and for this a critical nucleus size r_c has to be exceeded, (2) there must be an instability of the microstructure i.e. differences in dislocation density, and (3) at least at one side of the nucleus the boundary must be a mobile grain boundary i.e. a high angle boundary (for more details see section A3.5) (Gottstein and Mecking, 1985). The possibility that a strain free nucleus satisfies the prerequisites as stated above increases with increasing dislocation density (Kocks, 1985). The new grain exhibits a low dislocation density because during nucleation and growth of the nucleus dislocations are swept into the moving tilt wall.

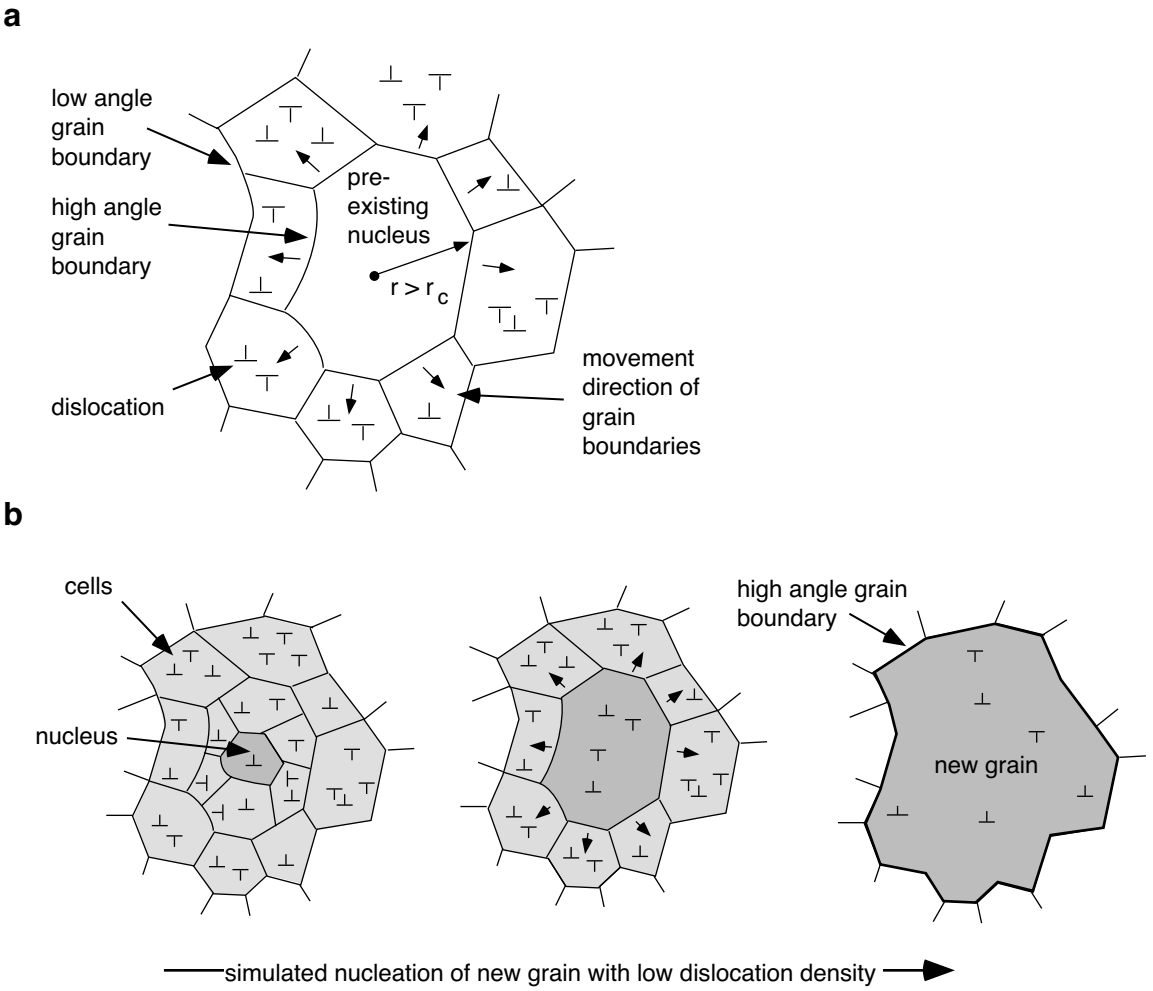

Figure A8 *Schematic illustration of the mechanism recrystallization by nucleation.* ***(a)*** *recrystallization nucleus with growth potential in a deformed structure (modified after Gottstein and Svindlermann, 1999). A nucleus can only grow if the total free energy decreases during expansion of the nucleus. For this a critical nucleus size* r_c *has to be exceeded (Gottstein and Svindlermann, 1999).* ***(b)*** *Schematic illustration of recrystallization by nucleation as simulated in the Elle model.*

The mobility of dislocations, which is directly related to the growth rate of a nucleus is temperature dependent according to the general form

$$v_m = \beta \mid b \mid \kappa \exp \frac{\Delta G}{kT} \qquad \text{(Eq. A6)}$$

where v_m is the mean velocity of a dislocation segment, ΔG the Gibbs free energy of activation for the cutting or by-passing of an obstacle, β is a dimensionless, material dependent constant, $|b|$ the magnitude of the Burgers vector and κ the frequency of obstacle jumps (Frost & Ashby, 1983). According to Eq. A6 the boundaries of a new nucleus will sweep over its neighbouring grains at higher speed at higher temperature than at low temperature.

In ELLE_NUCLXX, the critical threshold value *RX* for the necessary energy at which a grain can nucleate is material and temperature dependent. According to Eq. A6 the possibility of a nucleus to successfully nucleate within a time step is higher at higher temperatures. In accordance with this relationship, the *RX* at a specific temperature is related to RX_{nucl}. RX_{nucl} is the base nucleation threshold value specific to a mineral species. *RX* is calculated in the following way:

$$RX = (RX_{nucl}) \bullet c/(\mathrm{T}+c) \qquad \text{(Eq. A7)}$$

where *c* is a constant and T the temperature. This formula ensures the general trend of decreasing *RX* with increasing T. If $F(\rho)$ (Eq. A4) > *RX* there is a certain probability (calculated according to $\mathbf{P_{action}}$ (Eq. A5)) that a nucleus which fulfils the three requirements for recrystallization by nucleation is present in a polygon (see above). The dislocation density of a newly nucleated grain is set to a specified low dislocation density value (ρ'_{nucl}) and a new randomly picked crystallographic orientation. The randomly picked orientation must satisfy the condition that the boundaries at all sides of the grain of the recrystallized grains are mobile, high angle boundaries. A new nucleus will only be able to grow if at least some of its boundaries are high angle boundaries (Fig. A8b). The position of subgrain boundaries does not change in this routine due to computational limitations. Therefore, all subgrain boundaries must be high angle boundaries to allow the ”successful” nucleation of a grain.

A3.5 Rotational recrystallization (ELLE_ROTXX)

Low angle boundaries, which are defined by a tilt wall, develop into high angle boundaries by progressive misorientation of stationary subgrain boundaries. Such high angle boundaries have a different structure than tilt walls. They are characterized by the independence of its structure from domains on either side of it and overlapping dislocation cores (Gottstein and Shvindlerman, 1999, and references therein). In geology, this process of progressive misorientation is referred to as rotational recrystallization (Guillopé and Poirier, 1979; Poirier, 1985). The transition from a low to a high angle grain boundary structure is thought to occur at a critical angle of misorientation δ that is specific to a mineral phase (Fig. A9; e.g. Gottstein and Mecking, 1985; Drury and Urai 1990).

ELLE_ROTXX distinguishes between subgrains and grains. If all sides of a polygon are classified as high angle boundaries, the polygon is recognized as a grain and not as a subgrain. The value of the critical angle between a high and low angle boundary (*MisorientAngle*) is specific to the mineral phase. Only the grain/subgrain attribute is changed (cf. section A2). No physical properties of the polygon are affected by this routine. The calculation of the misorientation is performed according to the procedure described by Randle (1995) and Lloyd et al. (1992) as this procedure is commonly used in grain boundary studies (e.g. Trimby et al., 1998; Fliervoet and White, 1995; Fliervoet et al., 1999).

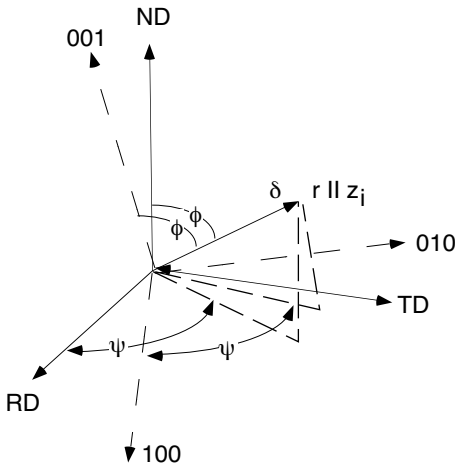

Figure A9 *Definition of the MisorientAngle δ between to crystals A {RD, TD, ND} and B {(100), (010), (001)} (modified after Gottstein & Svindlermann 1999).*

A3.6. Grain boundary migration (ELLE_GBM)

A positive driving force for grain boundary migration occurs if a grain boundary displacement results in a decrease of the total free energy of the system. The driving force is a combination of two separate forces. These are (a) the force resulting from the difference in stored, internal energy i.e. strain energy and (b) the difference in chemical potential between adjacent grains.

A deformed grain stores a certain amount of energy by the build-up of dislocations (e.g. Frost and Ashby, 1983 and references therein; Kocks, 1985; Barber, 1985). The higher the dislocation density the higher the stored energy according to

$$E_{stored} = \rho_{energy} \bullet A \bullet \rho \qquad \text{(Eq. A8)}$$

where ρ_{energy} is the energy of dislocations, ρ dislocation density and A the area.

The difference of dislocation density between two adjacent grains is a driving force for grain boundary migration. The grain boundary migrates towards the grain with the highest dislocation density to reduce the total local energy state of the system (Fig. A10). The area swept is devoid of dislocations as dislocations move into the moving grain boundary (Barber, 1985; Kocks, 1985).

The difference in chemical potential between grains occurs as a function of the surface free energy. The difference in grain boundary curvature between grains of different sizes result in a chemical potential gradients across the interface grain boundary according to the Gibbs-Thompson equation (e.g. Lewis and Randall, 1961):

$$\mu_i - \mu_i^0 = \frac{2\varepsilon V}{r} \times \zeta \qquad \text{(Eq. A9)}$$

where is ε the surface energy of the phase. The equation relates the chemical potential of component i at the surface of a spherical phase, radius r and molar volume V to that of a planar surface at the distance r form the centre of the crystal. A geometric factor ζ is applied to account in differences in grain shape.

Additionally, the surface energy has been shown to be anisotropic. Surface energy anisotropies are a function of the (a) the relative crystallographic orientation of the boundary i.e. tilt angle between two neighbouring grains (anisotropy A_{XX}) and (b) crystallographic orientation of the boundary (anisotropy A_{α}) (e.g. Urai et al. 1986; Grest et al., 1985; Gottstein and Shvindlerman, 1999).

In ELLE_GBM the simulation of grain boundary migration is performed by successive movement of each individual node present in the node network. The movement of an individual node consists of two components: (a) the node movement routine and (b) the calculation of the change in energy due to the movement of a node.

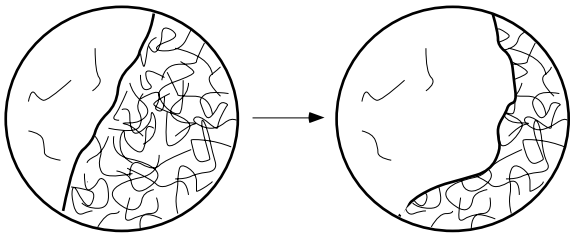

Figure A10 *Schematic diagram illustrating grain boundary migration due to energy differences derived from the energy of dislocations. The grain with low dislocation density migrates in the grain with high dislocation density to lower the total free energy of the system (modified after Passchier and Trouw , Fig. A17a).*

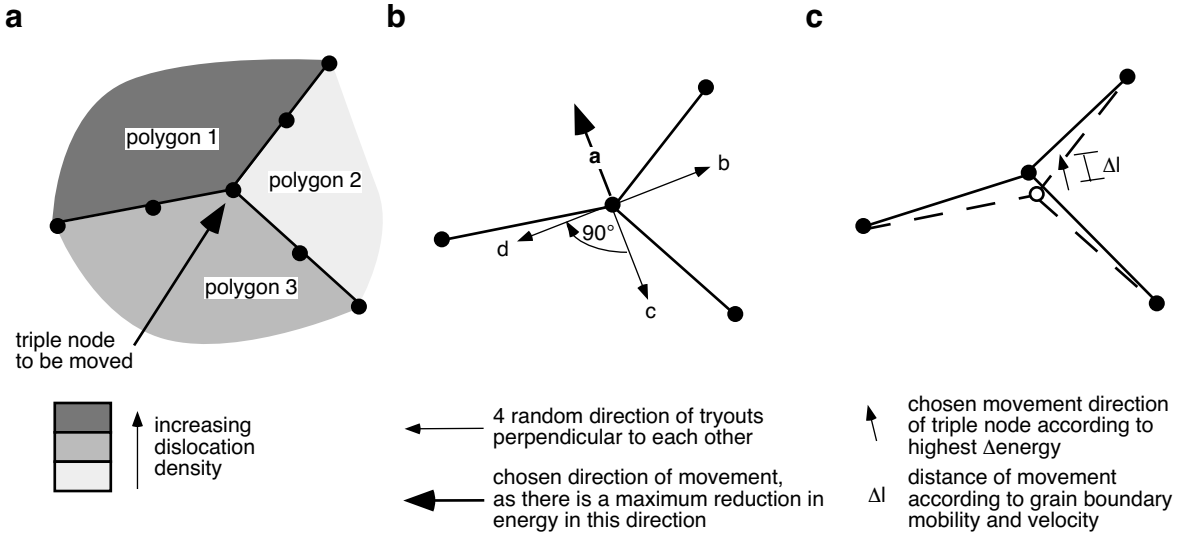

Figure A11 *Schematic diagram which illustrates the numerical procedure performed to achieve movement of one node according to the maximum reduction of energy.* ***(a)*** *Initial node-boundary-polygon configuration with different dislocation densities in different polygons.* ***(b)*** *Illustration of the randomly chosen four tryout directions;* ***(c)*** *resultant movement.*

In ELLE_GBM a small displacement of a node changes the total energy state by ΔE_{trial}. A small displacement vector p_{trial} of length D_{trial}, in a random direction is chosen and ΔE_{trial} is calculated. The length D_{trial} is calculated according to a defined fraction d (usually 0.01) of the *SwitchDistance* between two nodes

$$D_{trial} = SwitchDistance \bullet d \qquad \text{(Eq. A10)}$$

The calculation of ΔE_{trial} is repeated for another three displacements, each time rotating the trial displacement vector p_{trial} by 90 degrees. The displacement vector p_{trial} along which a node displacement results in the largest reduction of the local energy state is taken as the movement vector for the actual migration of the node concerned (Fig. A11). Once this movement vector p has been chosen the amount of true displacement D of the node is calculated and the node moved by this displacement along p.

To choose the relevant p_{trial} the change in energy due to the displacement D_{trial} in the p_{trial} direction must be calculated. In ELLE_GBM the calculation of the change in energy is divided in two main components. These are the change strain energy stored in adjacent polygons (ΔE_{ρ}) and the change in surface energy (ΔE_{ϕ}). These values are calculated according to the displacement of the node by D_{trial}.

To calculated the trial change in energy due to dislocation density ($\Delta E_{\rho-trial}$) first the "real world" area (*initialArea*) for each polygon adjacent to a double or triple node under consideration is calculated according to

$$initialArea = Elle\_area \bullet l_{scale}^{2} \qquad \text{(Eq. A11)}$$

where *Elle_area* is the area stored in the Elle file. The dislocation density *ρ'(initial)* stored in the Elle file of each polygon is retrieved. It is assumed that the dislocation density within one polygon is homogeneous, therefore the initial energy due to dislocations $E_{\rho}(initial)$ of each polygon can be calculated according to

$$E_{\rho}(initial) = \rho_{energy} \bullet initialArea \bullet \rho'(initial) \bullet \rho_{scale} \qquad \text{(Eq. A12)}$$

where ρ_{energy} is the energy of dislocations, *ρ'(initial)* the dislocation density stored in the Elle data file and ρ_{scale} the dislocation density scaling factor. Then the node position is changed according to D_{trial} and p_{trial}. This new node position results in a change in the areas of the polygons concerned. If the new area (*newArea*) of the polygon is smaller than the *initialArea* no change in dislocation density and therefore no energy difference will be present. If *newArea* > *initialArea* the dislocation density of the polygon is assumed to change according to the following equation.

$$\rho'(new) = (initialArea/newArea) \bullet \rho'(initial) \qquad \text{(Eq. A13)}$$

This change in dislocation density with increasing area, results in an decrease of the dislocation density of a "growing" grain. This calculation is valid under the assumption that the swept area is dislocation free. This is reasonable, because dislocations that were present in the swept area before movement of the node accumulate in the grain boundary (Kocks, 1985). For a "growing" polygon where *newArea* > *initialArea* the new energy $E_\rho(new)$ is calculated according to

$$E_\rho(new) = \rho_{energy} \bullet newArea \bullet \rho' \bullet \rho_{scale} \qquad \text{(Eq. A14)}$$

The difference in stored energy $\Delta E_\rho(polygon)$ of a "growing" polygon is calculated by

$$\Delta E_\rho(polygon) = E_\rho(initial) - E_\rho(new) \qquad \text{(Eq. A15)}$$

The total change in $\Delta E_{\rho-trial}$ is the sum of the $\Delta E_\rho(polygon)$ of the polygons involved (Note: for a polygon where *newArea* < *initialArea* $\Delta E_\rho(polygon) = 0$).

$$\Delta E_\rho = \Sigma E_\rho(polgon) \qquad \text{(Eq. A16)}$$

In ELLE_GBM the second driving force considered is the change in surface energy due to the movement of a node. The calculation of the surface energy change (ΔE_ϕ) has 3 components. These are (a) surface energy due to length of the boundary segments involved $E_{length,}$ (b) anisotropy A_{XX} of this surface energy due to relative crystallographic orientation of two adjacent grains and (c) anisotropy A_α of the surface energy due to orientation of the boundary with respect to its crystallographic orientation (Bons et al., in press). In two dimensions E_{length} is at a minimum if boundaries are straight and intersections angle are 120°. In E_{length} calculations, the initial and end length of the boundary segments that change their length due to the movement of a node is calculated. Assuming an isotropic surface energy, the energy state is the length of the segments multiplied by the surface energy.

For the example, of a double-node in Fig. A12 with bounding two segments of lengths l_1 and l_2, the energy E_{length} is generally given by

$$E_{length} = \Gamma \bullet (l_1 + l_2) \qquad \text{(Eq. A17)}$$

where Γ is the surface energy and l_1, l_2 the lengths of the two segments next to the node. The movement over vector D_{trial} results in a change in segment lengths l_1 and l_2 to new lengths (l'_1, l'_2).

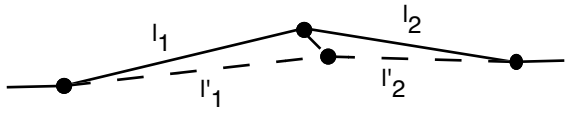

Figure A12 *Schematic diagram illustrating the parameters used for the calculation of surface energy.*

In ELLE_GBM the initial and new segment lengths E_{length} for the boundaries concerned is calculated. The change in energy (ΔE_{length}) is the difference between the two. This part of the routine is based on the model of P. D. Bons (1993) and Jessell et al. (2001). And it has been shown to be a valid for grain boundary energy driven grain boundary migration (Bons, 1993; Jessell et al., 2001; Bons et al., in press). The anisotropy of surface energy of a grain boundary is low if the angle of crystallographic orientation between two adjacent grains is low and high at high angles (Fig. A13). Read and Shockley (1950) showed that for a symmetrical tilt boundary with tilt angle φ, the surface energy σ_b per unit area is in a general form

$$\sigma_b = \varphi\,(K \bullet \ln \varphi) \qquad \text{(Eq. A18)}$$

where K is a material constant. In ELLE_GBM, the relationship between the isotropic surface energy (Γ_i) and anisotropic surface energy (Γ_a) due to the angular relationship the crystallographic misorientation of the c-axis between two adjacent crystals A and B (tilt angle Π) on either side of the grain boundary is assumed to follow the general form

$$\Gamma_a = \Gamma_i \bullet \text{ xx\_factor}(\Pi) \qquad \text{(Eq. A19)}$$

where *xx_factor* ranges between 0 and 1 and is a function of tilt angle Π . The values of *xx_factor* are derived from a file. In this file the *xx_factor* values for specific tilt angle Π ranges are listed. This part of ELLE_GBM is an implementation of an existing code written by P. D. Bons and M. W. Jessell.

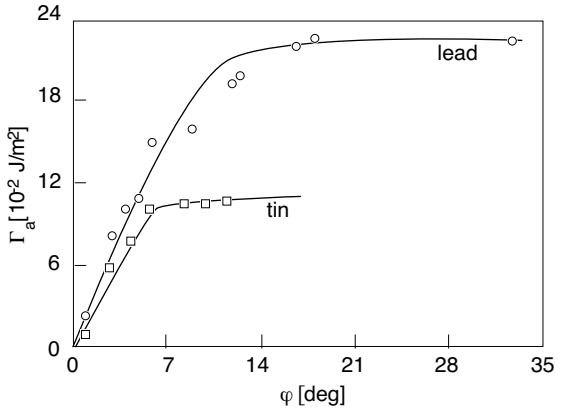

Figure A13 *Surface energy Γ_a of grain boundaries with a specific tilt angle between two adjacent grains (φ). Open dots and squares signify measurements of specimen of lead and tin respectively (modified after Gottstein and Svindlerman, 1999).*

In ELLE_GBM the anisotropy of the surface energy A_α relates the angular relationship between the orientation of the grain boundary and crystal lattices. A_α is a function of the five angles α_1, α_2, α_3, α_4, α_5 which define the orientation of a boundary and the lattices of the adjacent crystals on either side of the boundary:

$$A_\alpha = F(\alpha_1, \alpha_2, \alpha_3, \alpha_4, \alpha_5) \quad \text{(Eq. A20)}$$

Different functions which describe A_α can be chosen depending on the character of anisotropy to be modelled. Details of the assumption for different surface energy anisotropies and possible functions to be chosen from are described in detail in Bons et al. (in press). Again, this part of ELLE_GBM was written by P. D. Bons and its applicability to the microstructural development of metals and crystalline analogue materials has been shown in Bons et al. (in press).

The following equation is used to draw together the effect of the three components E_{length}, A_{XX} and A_α that influence the surface energy of a boundary segment,

$$E_\phi = l \bullet xx\_factor \bullet \Gamma \bullet A_{XX} \bullet l_{scale} \quad \text{(Eq. A21)}$$

where l is the length of boundary and Γ a predefined surface energy. The change in energy ($\Delta E_{\phi-trial}$) is the difference between the energies E_ϕ calculated for the initial node position and its position after D_{trial} along vector p_{trial}.

In ELLE_GBM the total energy change $\Delta E_{\boldsymbol{trial}}$ which would arise from node movement with D_{trial} along p_{trial} is calculated according to

$$\Delta E_{trial} = \Delta E_{\phi-\boldsymbol{trial}} + \Delta E_{\rho\text{-}trial} \quad \text{(Eq. A22)}$$

where ΔE_ϕ is calculated according to Eq. A21 and ΔE_ρ according to Eq. A16.

ΔE_{trial} is calculated for each of the four trial node positions. Vector p for which ΔE_{trial} is the highest is taken as the valid vector for the true movement of the node. Once p is chosen the true displacement D in direction of the chosen direction vector p can be calculated according to

$$D = v_{node} \bullet \mathrm{t_{scale}} \quad \text{(Eq. A23)}$$

whereby v_{node} is the velocity of node movement and $\mathrm{t_{scale}}$ the time scaling factor. The rate at which grain boundary migration i.e. the velocity of the boundary movement occurs depends on the mobility of the boundary and the value of the driving force according to the general relationship

$$\mathrm{v} \propto \mathrm{M} \bullet \mathrm{F} \quad \text{(Eq. A24)}$$

(Frost and Ashby, 1983 and references therein) where v is the velocity, M the mobility and F the driving force for grain boundary migration.

In ELLE_GBM, this means

$$v_{node} = GBMob \bullet \Delta E \quad \text{(Eq. A25)}$$

where ΔE is the calculated change in energy due to the D_{trial} along the chosen vector p and *GBMob* the mobility. Once the *GBMob* is known the velocity of the node v_{node} can be calculated.

To calculate the value of *GBMob* the following considerations have to be taken into account. In general, the grain boundary mobility M is mainly function of temperature and material (Fig. A14; Frost and Ashby, 1983; Gottstein and Shvindlermann, 1999 and references therein). Additionally, the amount of impurities (Olgaard and Evans, 1986; Randle et al., 1986) are important for the effective grain boundary mobility. Assuming no impurities the relationship of M to temperature follows a general Arrhenius equation of the form

$$M = M_{0\bullet}\, e^{(-H/(B\bullet T))} \qquad \text{(Eq. A26)}$$

(e.g. Frost and Ashby, 1983; Gottstein and Svindlerman, 1999, and references therein) where H is the activation energy, B is the Boltzmann constant, and M_0 a 'base mobility' specific to a material.

In ELLE_GBM, the grain boundary mobility is calculated according to

$$GBMob = GBMob_0 \bullet e^{(-QGBM/(B \bullet t))} \qquad \text{(Eq. A27)}$$

where *GBMob* is the grain boundary mobility, *QGBM* is the activation energy, B is the boltzmann constant and $GBMob_0$ a "base mobility" specific to a material. The direct relationship of grain boundary velocity, grain boundary mobility and driving force assumes no variations due to impurities and drag effects. Additionally, it is assumed that the intensive variables pressure, temperature and magnetic field show no gradients in the experiments. They can therefore be neglected.

Now, the new position of the node can be calculated using v (calculated by Eq. A25 and Eq. A27), D (calculated by Eq. A23) and the chosen vector p.

In ELLE_GBM a number of assumptions and approximations are made and therefore the relevance of such a calculation of the node movement had to be tested in several ways. The validity the general mode of determination of the relevant movement direction (trial vectors p_{trial}; Fig. A11) is discussed in Bons et al. (in press).

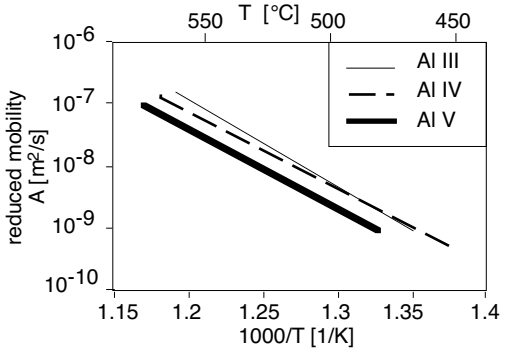

Figure A14 *Dependence of the mobility on material and temperature. Depicted is the reduced mobility A for 40.5° <111> tilt boundaries in differently pure Al: Al III, Al IV and Al V have an impurity content of A6 ppm, 4.9 ppm and 7.7 ppm, respectively (modified after Gottstein & Svindlermann 1999).*

Several tests were performed simulating the microstructural evolution of a fabric due to grain boundary migration. ELLE_GBM was divided into two individual routines (ELLE_DISLOC, ELLE_SURF). In ELLE_DISLOC exclusively the change in stored energy due to dislocations is considered for the driving force calculation for grain boundary migration.

In ELLE_SURF exclusively the change in surface energy due to the change in length (E_{length}) and the anisotropy A_{xx} of a grain boundary are considered. The change in microstructure of a combination of ELLE_DISLOC and ELLE_SURF show very similar results as simulations using ELLE_GBM which assumes $A_{\alpha} = 1$. In addition, results of several simulations with identical parameters and initial microstructure, shown that simulations are reproducable.

A3.6. Recovery (ELLE_RECOVERY)

Deformed crystals tend to remove lattice defects that are not in thermodynamic equilibrium in order to lower the energy of its system. In the metallurgical sense, recovery results in low energy dislocation structures by either dislocation annihilation or locally rearrangement in cell and subgrain walls. The amount of annihilation per unit area and time step depends on both material and temperature (Hu, 1963; Kocks et al. 1975; Kocks, 1985; Gottstein and Shvindlerman, 1999 and references therein). Recovery that results in the rearrangement of dislocations is simulated by the subgrain formation routine (ELLE_SPLIT; section A3.3).

ELLE_RECOVERY exclusively simulates recovery that describes the time- and temperature-dependent annihilation of non-geometrically necessary dislocations within a crystal. In the routine the dislocation density of each grain or subgrain is reduced per time step according to a recovery factor RF. First the temperature dependent *RF* is calculated according to:

$$RF = e \bullet RF_{base} + ((1\text{-}e) \bullet RF_{base} \bullet f/(\mathrm{T}+f) \qquad \text{(Eq. A28)}$$

where RF_{base} is the base recovery factor specific to a mineral species, e a constant between 0 and 1 and f a constant. This formula is arbitrary. We know, though, that the recovery rate is a function of the mineral species and some form of 1/T, therefore we regard the formula above as a reasonable approximation of the process active in nature (Kocks, 1985). The new dislocation density is then calculated according to

$$\rho'(new) = \rho'(initial) \bullet RF \qquad \text{(Eq. A29)}$$

This type of equation ensures a progressive decrease in dislocation density provided no new dislocations are generated (Fig. A15).

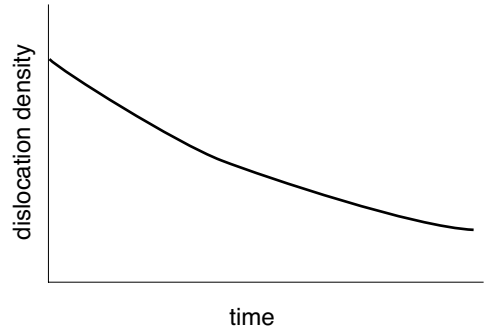

Figure A15 *Schematic graph illustrating the decrease in dislocation density with time. It is assumed that the only active process that changes in dislocation density is recovery.*

A3.7 Calculation of viscosity (ELLE_VISCOSITY)

The rate at which crystals deform viscously depends on the applied stress and the viscosity of the grain.

$$\dot{\gamma} \propto \frac{\sigma}{\eta} \qquad \text{(Eq. A30)}$$

The viscosity of a grain is largely a function of the mineral species, dislocation density of the crystal, temperature and presence of a fluid phase. Fluid presence enhances dislocation glide and climb by hydraulic weakening (Kronenberg & Tullis, 1984;, Tullis & Yund 1988, 1989; Post et al., 1996).

Dislocations interact with each other, and since many dislocations must move distances which are large compared to their spacing to achieve macroscopic flow, dislocation interactions are of fundamental importance for plasticity and viscosity (e.g. Kocks 1976, 1985; Frost and Ashby, 1983 and references therein) (see also A3.2). The general relationship between strain rate and dislocation density assuming dislocation glide as the main deformation mechanism is given by the Orowan's equation

$$\dot{\gamma} = \rho \mid b \mid \bar{v} \qquad \text{(Eq. A31)}$$

where |b| is the magnitude of the Burgers' vector and v the average velocity determined almost entirely by the time to overcome obstacles. The velocity of dislocations in a polycrystal is frequently determined by the strength and denstiy of the dicrete obstacles it contains. If it is assumed that the activation energy required to overcome the obstacle is the rate limiting factor for the deformation of a material, which means that the obstacle is "strong", the strain rate is related to dislocation density and stress in the following manner.

$$\dot{\gamma} \propto \frac{\sigma}{\sqrt{\rho}} \qquad \text{(Eq. A32)}$$

(Frost and Ashby, 1983). Therefore, the viscosity is related to the dislocation density according to the general relationship

$$\eta \propto \text{sqrt}(\rho) \qquad \text{(Eq. A33)}$$

This is in the accordance to the described "work-hardening" phenomenon (section A3.2; Kocks, 1976; Kocks et al. 1975). The term work hardening describes an increased resistance to dislocation movement with increasing dislocation density. Thus, a crystal requires additional stress to move further dislocations.

In ELLE_VISCOSITY (due to computational limitations) it is assumed that the material is viscous, rather than plastic. The following viscosity calculation was used

$$\eta = (\eta_{base} + Fluid\_Factor \bullet \text{SQRT}(\rho')) \qquad \text{(Eq. A34)}$$

where η_{base} is the "base" viscosity specific to a mineral species. This equation ensures the dependence of viscosity (η_{base}), dislocation density and the degree of hydraulic weakening i.e. value of *Fluid_Factor* (Fig. A16).

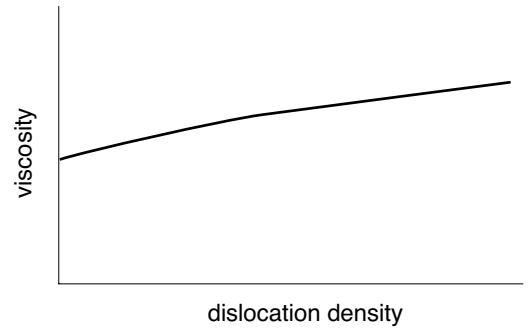

Figure A16 *Schematic graph illustrating the general relationship between viscosity and dislocation density as assumed in Elle calculations. The fluid activity is assumed to be constant.*

A4 Data storage, display, statistics and clean-up of computationally problematic mesh geometries

A4.1 Data storage

At each time step an Elle data file is automatically stored. The data file gives a full description of the geometry of the simulated microstructure. It also stores for each polygon the grain number it belongs to, its mineralogy, viscosity, dislocation density, crystallographic orientation (Euler angles), strain attributes, age, the number of recrystallization cycles it was involved in and if it is a subgrain or a not. Additionally, for each node the stress values are stored.

A4.2 Display of Elle data (SHOWELLE)

With the display program SHOWELLE the data stored in the Elle data file, such as the position of nodes and connection boundaries, as well as polygon and the calculated boundary attribute "angle of misorientation (see section A3.5) can be visualized in colour or in grey scale.

A4.3 Statistics (ELLE_STATS)

A separate routine ELLE_STATS generates a statistics file to keep track of the microstructural evolution of a microstructure for each time step. It analyses the data given in the data file and writes results to a statistics file. The following data are stored: total number of polygons, polygon number, polygon area, polygon mineral attribute, age, cycle of recrystallization, total number of grains, grain number, grain area, length of grain boundaries according to different angle of misorientation categories, total grain boundary length. A grain is defined as the sum of polygons, which are adjacent to each other and exhibit no high angle boundaries between each other. The same procedure as used for the rotational recrystallization routine (section A3.5) was used to calculated the angle of misorientation. A grain shape analysis (Panozzo, 1983, 1984) is performed using the algorithm written by P. D. Bons (Bons, 1993). This method (Panozzo, 1983, 1984) assumes that the average grain shape preferred orientation (SPO) can be described by an ellipse with an aspect ratio (R_a) and an orientation of the long axis of the ellipse (α) using the orientation of the grain boundaries. Only grain boundaries that did not touch the network boundaries were used for the calculation. Output of the analyses are the ratio of long to short shape axis of the average fitted ellipsoid, maximum angle of long shape axis, minimum angle of long shape axis and accuracy of shape related calculations.

A4.4 Clean-up of computationally problematic mesh geometries (ELLE_CHECKANGLE)

ELLE_CHECKANGLE is a routine to "clean-up" topologically problematic mesh geometries. BASIL has problems triangulating regions with very sharp angles or very small areas which may develop. If either of these problems occurs, BASIL will usually run out of memory due to the creation of many unnecessary small triangles which are used in BASIL. Therefore, a routine was developed to get rid of these sharp angles and very small areas (Fig. A17). The threshold values at which this routine is applied are minimum angle *MinAngle* and the area of a triangle with sides of the length of the minimum node separation (*MinNodeSep*).

Such a routine is justified as in natural examples in which very sharp angles between grain boundaries are not observed and very small grains are rare. This is in accordance to thermodynamic instability of very small angles and very small grains according to Eq. A9. High curvature, hence high radii, result in high driving forces to move the boundary towards the centre of curvature.

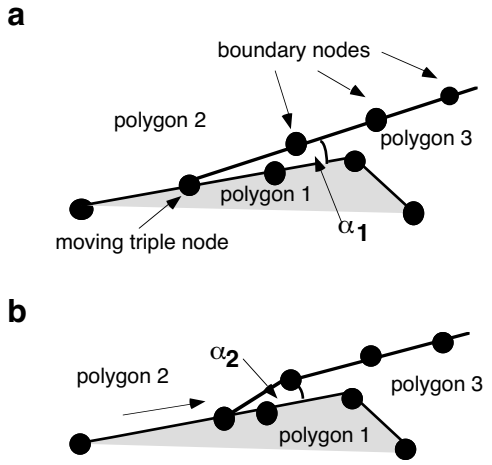

Figure A17 *Schematic diagram illustrating the effect of the clean-up routine.* ***(a)*** *In the routine sharp angle between two grain boundaries (α_1) are recognized and* ***(b)*** *one node is moved along one grain boundary. The distance between the original node position and the new node position is chosen in such a way that the resultant enclosing angle $\alpha_2 > MinAngle$. The decision which node is moved along which boundary is random if all polygons are polygons of the same mineral species. If one of the polygons (e.g. polygon 1) has a different mineralogy than the other polygons involved, node is moved along the boundary between polygons of the same mineral species.*

Table A1 *Used symbols*

a	constant in ELLE_TBH	-
A	area of grain	m^2
Elle_area	dimensionless area of polygon stored in Elle file	-
MinAngle	Minimum angle allowed in between boundary segments	¡
MisorientAngle	angle below which polygon boundaries are regarded as subgrain boundaries	¡
MinArea	minimum area of new subgrain	mm^2
MaxArea	maximum area of new subgrain	mm^2
initialArea	area of polygon before node movement	m^2
newArea	area of polygon after node movement	m^2
A_{XX}	anisotropy of surface energy due to tilt angle between boundaries	-
A_α	anisotropy of surface energy due to crystallographic orientation of boundary in ELLE_GBM	-
b	constant in ELLE_TBH	-
B	Boltzmann constant	JK^{-1}
|b|	magnitude of the Burgers vector	-
c	constant in ELLE_NUCLXX	-
CRSS	critical resolved shear stress used in ELLE_TBH	-
C	constant of proportionality of a fractal set	-
d	factor used to calculated distance for trial displacment	-
D	fractal dimension	-
D	chosen displacement for node movement in ELLE_GBM	m
D_{trial}	trial displacement of node used in ELLE_GBM	m
e	constant in ELLE_RECOVERY	-
ework	work term in ELLE_TBH	-
E_{stored}	strain energy stored in grain	Jm^{-2}
E_ρ	energy due to dislocation density in ELLE_GBM	Jm^{-2}
$E_{\rho(polygon)}$	energy of a polygon due to dislocation density in ELLE_GBM	Jm^{-2}
$E_{\rho\text{-}trial}$	trial energy due to dislocation density in ELLE_GBM	Jm^{-2}
E_ϕ	overall surface energy in ELLE_GBM	Jm^{-2}
E_{trial}	trial energy in ELLE_GBM	Jm^{-2}
E_{length}	surface energy due to length of boundary in ELLE_GBM	Jm^{-2}
f	constant in ELLE_RECOVERY	-
F	driving force	Jm^{-3}
Fluid_Factor	factor describing the presence of H_2O at grain boundary	-
F(ρ)	available energy for subgrain formation	Jm^{-2}
F_{xy}	ratio of number of values in the highest frequency bins of histograms of x-direction and y-direction of gbd-plots	-
gbd-plots	grain boundary distance plots	-
ΔG	Gibbs free energy of activation for by-passing of an obstacle	Jm^{-2}
GBMob	grain boundary mobility in ELLE_GBM	$m^2\ s^{-1}J^{-1}$
$GBMob_0$	base grain boundary mobility in ELLE_GBM	$m^2\ s^{-1}J^{-1}$
H	activation energy	Jm^{-2}
i	chemical component	-
l	length of boundary segment in ELLE_GBM	m
l_{scale}	length scaling factor	m
n	stress exponent of power law flow	-
N_n	number of objects of fractal set	-
O	given vector for splitting direction in ELLE_GBM	
p	chosen vector for node displacement used in ELLE_GBM	-
p_{trial}	random vector for trial walks used in ELLE_GBM	-
P	pressure	kbar
$\mathbf{P_{action}}$	probability function in ELLE_GBM	-
QGBM	grain boundary activation energy	$Jmol^{-1}$
r_n	linear dimension of a fractal set	-
RF_{base}	recovery factor (material dependent) in ELLE_GBM	-
RF	Effective recovery factor in ELLE_GBM	-
R_a	aspect ratio of ellipse calculated from orientation of grain boundaries	-
R_a	aspect ratio of strain ellipse	-
R_{gbl}	ratio low/high angle boundary length per unit area	-
RX	energy threshold value for recrystallization by nucleation in ELLE_GBM	Jm^{-2}
RX_{nucl}	initial energy threshold value for recrystallization by nucleation (material dependent) in ELLE_GBM	Jm^{-2}
R_Φ	ratio of initial to recrystallized grain size	-
M	grain boundary mobility in general sense	$m^2\ s^{-1}J^{-1}$
M_0	base grain boundary mobility specific to a mineral species	$m^2\ s^{-1}J^{-1}$
MinNodeSep	minimum node separation	m^2
MaxNodeSep	maximum node separation	m^2
Switch	maximum distance between joint triple nodes	m^2
t	time	s
t_{scale}	time scaling factor	s
T	temperature	¡C
Th_{split}	energy threshold for splitting in ELLE_GBM	Jm^{-2}
r	radius of a sphere	m
V	molar volume of phase	$molcm^{-3}$
v	velocity of grain boundary migration - general	ms^{-1}
v_m	mean velocity of a dislocation segment	ms^{-1}
v_{node}	velocity of node movement in ELLE_GBM	ms^{-1}
W_n	kinematic vorticity number	-
xx_factor	crystallographic misorientation factor in ELLE_GBM	-
α	angle between the long principal axis of the calculated ellipse and the shear plane	s
β	angle between the long principal axis of the strain ellipse and the shear plane	-
Δs	displacement per time step	-
Δγ	strain per step	-
δ	Material constant (Eq. 3.2)	-
Π	Tilt angle of c-axis of adjacent crystals in ELLE_GBM	-
ε	surface energy of phase (Gibbs-Thompson equation)	-
	strain rate	s^{-1}
γ	finite strain	-
κ	frequency of obstacle jumps	s^{-1}
ρ	density of mobile dislocations	m^{-2}
ρ	dislocation density of a polygon stored in Elle data file	m^{-2}
ρ (initial)	initial dislocation density of a polygon	m^{-2}
ρ (new)	new dislocation density of a polygon	m^{-2}
ρ_{energy}	dislocation energy	Jm^{-2}
ρ_{nucl}	dislocation density of newly nucleated grain	m^{-2}
ρ_{scale}	dislocation density scaling factor	m^{-2}
τ_{scale}	stress scaling factor	Pa
Γ	surface energy	Jm^{-2}
Γ_i	isotropic surface energy	Jm^{-2}
η	viscosity	Pa s
η_{base}	base viscosity	Pa s
μ	chemical potential	-
ζ	geometric factor (Gibbs-Thompson equation)	-
φ	tilt angle between two adjacent grains	¡
ν	frequency of obstacle jumps	s^{-1}
σ	stress	Pa
σ_b	grain boundary energy due to tilt angle between boundaries - general	Jm^{-2}